Direct Measurement of the Magnetocaloric Effect in $\mathbf{La(Fe,Si,Co)_{13}}$ Compounds in Pulsed Magnetic Fields

M. Ghorbani Zavareh,[1,2,*] Y. Skourski,[1] K. P. Skokov,[3] D. Yu. Karpenkov,[3,4] L. Zvyagina,[1] A. Waske,[5] D. Haskel,[6] M. Zhernenkov,[7] J. Wosnitza,[1,2] and O. Gutfleisch[3]

[1]*Hochfeld-Magnetlabor Dresden (HLD-EMFL), Helmholtz-Zentrum Dresden-Rossendorf, 01314 Dresden, Germany*
[2]*Institut für Festkörperphysik, TU Dresden, 01062 Dresden, Germany*
[3]*Technische Universität Darmstadt, Institut für Materialwissenschaft, 64287 Darmstadt, Germany*
[4]*NUST MISiS, Leninskiy prospect 4, 119049 Moscow, Russia*
[5]*IFW Dresden, Institute for Complex Materials, 01171 Dresden, Germany*
[6]*Advanced Photon Source, Argonne National Laboratory, Argonne, Illinois 60439, USA*
[7]*National Synchrotron Light Source II, Brookhaven National Laboratory, Upton, New York 11973, USA*
(Received 26 June 2017; published 28 July 2017)

We report on magnetization, magnetostriction, and magnetocaloric-effect measurements of polycrystalline $\mathrm{LaFe_{11.74}Co_{0.13}Si_{1.13}}$ and $\mathrm{LaFe_{11.21}Co_{0.65}Si_{1.11}}$ performed in both pulsed and static magnetic fields. Although the two compounds behave rather differently at low fields (~ 5 T), they show quite similar values of the magnetocaloric effect, namely a temperature increases of about 20 K at high fields (50–60 T). The magnetostriction and magnetization also reach very similar values here. We are able to quantify the magnetoelastic coupling and, based on that, apply the Bean-Rodbell criterion distinguishing first- and second-order transitions.

I. INTRODUCTION

Magnetocaloric materials are the basis for a solid-state alternative to conventional compressor-based refrigeration at ambient temperature [1–4]. The rapidly developing class of magnetic refrigerators, heat pumps, and air-conditioning units based on these materials is considered to be environmentally friendly, silent, compact, and energy efficient [5]. The magnetic-cooling technology is based on materials exhibiting magnetic or magnetostructural phase transitions which are responsible for a large entropy change in the magnetic and structural subsystems upon the application or removal of an external magnetic field. This, in turn, results in a large magnetocaloric effect (MCE) [6].

The magnetocaloric effect is defined as the change of the temperature T and entropy S caused by the variation of an applied magnetic field. Under adiabatic conditions, S remains constant and the magnetocaloric effect can be characterized quantitatively by the observed adiabatic temperature change ΔT_{ad}. Alternatively, by keeping T constant during a field sweep (isothermal conditions), the magnetocaloric effect results in a heat transfer Q between the sample and the environment. Thereby, $Q = T \Delta S_m$, where ΔS_m is the isothermal magnetic-entropy change [7,8].

Both, ΔT_{ad} and ΔS_m comprehensively characterize magnetocaloric materials in terms of their potential application in magnetic refrigeration [9]. However, experimental data on ΔT_{ad} are still rather scarce in the literature. Mostly, the MCE is determined by measuring the isothermal, $M(H)_T$, or isofield, $M(T)_H$, magnetization with the subsequent calculation of $\Delta S_m(T)$ by using Maxwell relations. ΔT_{ad} and ΔS_m can also be extracted indirectly from S-T diagrams determined by the use of temperature-dependent heat-capacity data measured in different magnetic fields [10]. However, the conventional S-T diagrams describe states at thermal equilibrium, which for materials with first-order transitions are challenging to determine due to metastability and hysteresis. Since in a magnetic refrigerator the magnetocaloric materials usually are magnetized and demagnetized very quickly, the standard equilibrium S-T diagrams are only of limited use [11,12].

Indeed, the typical thermal-cycle design frequency of a magnetic refrigerator is in the range of 1–10 Hz (corresponding to a magnetic-field change rate of 2–50 T/s), whereas in the literature mainly reports on steady-field experiments are found with typical field-change rates of 0.01 T/s determined by the use of superconducting magnets. In order to determine the MCE near real operational conditions it is necessary to measure directly adiabatic temperature changes by using fast-sweeping magnets, such as standard electromagnets or assemblies of permanent magnets (e.g., nested Halbach cylinders). These allow us to measure ΔT_{ad} at frequencies up to 1 Hz with magnetic-field changes of up to 2 T/s [13,14].

In this work, we report on measurements of ΔT_{ad} in pulsed magnetic fields which provide us with a comprehensive access to the dynamic MCE and the high-field

[*]Present Address: Max Planck Institute for Chemical Physics of Solids, 01187 Dresden, Germany.

properties of materials with first- and second-order transitions. This allows us to investigate dynamic effects of magnetic refrigerants with relevant frequencies. Nondestructive pulsed magnets have typical pulse durations of 10–100 ms, which perfectly match the envisioned operation frequencies of magnetic refrigerators. Thereby, the magnetic-field change can be as fast as 1000 T/s.

Another important issue we are addressing in this paper is tuning the system between first- and second-order transitions. Often phase transitions from the paramagnetic (PM) to the ferromagnetic (FM) state are of second order. Such reversible transitions are accompanied by rather modest magnetocaloric effects. In contrast, some materials show first-order transitions when entering the FM state in applied magnetic fields. Thereby, abrupt volume changes occur at the critical temperature, resulting in rapid magnetization changes. As a result, large field-induced heating and cooling effects are observable, which make these materials very promising magnetocaloric refrigerants.

The big advantage of materials with first-order transitions is the relatively small magnetic field needed for switching between the PM and FM states. This allows the usage of permanent magnets in magnetic-cooling devices. On the other hand, a severe drawback is the thermal and magnetic hysteresis at the first-order transition. This drastically reduces the MCE when applying fields under cycling conditions [11,15–17]. Strong research efforts are directed towards materials design leading to reduced hysteresis.

In some materials we can shift the transition from first to second order by adjusting their composition slightly. An important goal is to reach the tricritical point [18,19] where the first-order transition becomes second order. This allows us to utilize the entropic benefits of the first-order transition without the reduction of the MCE due to hysteretic losses.

La(Fe, Si)$_{13}$-based compounds (with cubic NaZn$_{13}$-type structure) are among the most promising magnetocaloric materials. They show a large magnetocaloric effect and have been widely studied in quasistatic magnetic fields from the perspective of fundamental and applied research [20–22]. ΔT_{ad}, ΔS_m, and the Curie temperature T_C of La(Fe, Si)$_{13}$ alloys can be widely adjusted by small additions of other elements such as H or Co. The addition of Co also alters the nature of the magnetic phase transition from first to second order. La(Fe$_x$Si$_{1-x}$)$_{13}$ offers a unique combination of large ΔS_m of up to 30 JK^{-1} kg^{-1} in field changes of the order of 5 T coupled with remarkably small hysteresis. In this work, the alloys LaFe$_{11.74}$Co$_{0.13}$Si$_{1.13}$ and LaFe$_{11.21}$Co$_{0.65}$Si$_{1.11}$ are chosen for the investigation of the dynamic MCE in magnetic fields up to 60 T. We apply the theory proposed by Bean and Rodbell [23] to discriminate first- and second-order transitions. The Co-poor alloy shows a pronounced first-order transition at 198 K, whereas the Co-rich compound exhibits a second-order transition at 256 K.

II. EXPERIMENTAL

We investigate the magnetocaloric properties of commercial samples produced by Vacuumschmelze GmbH & Co. KG. The LaFe$_{11.74}$Co$_{0.13}$Si$_{1.13}$ and LaFe$_{11.21}$Co$_{0.65}$Si$_{1.11}$ samples are produced using a powder metallurgical route (reactive sintering) which consists of five basic steps: powder manufacture, powder blending, compacting, sintering, and machining [24,25].

Measurements of ΔT_{ad} in magnetic fields up to 1.93 T and field-sweep rates up to 2 T s^{-1} are performed in a dedicated experimental setup using permanent magnets in a Halbach-cylinder assembly [13]. The magnetic field is measured by a Hall probe. The temperature change of the sample is monitored with an accuracy better than ± 0.01 K using a Copper-Constantan (T-type) thermocouple. The samples are prepared as a stack of two equally shaped ($0.3 \times 5 \times 10$ mm) plates with the thermocouple placed in between. In order to reduce the influence of demagnetization effects all samples are measured with the magnetic field applied parallel to the 10-mm sample edge.

The isothermal magnetization and magnetic susceptibility up to 14 T are measured by using a physical properties measurement system (PPMS 14, Quantum Design) with vibrating sample magnetometer option.

In order to determine the compressibility, high-pressure x-ray diffraction (XRD) experiments are performed at the HP-CAT beam line 16-BM-D of the Advanced Photon Source using a Mao-type symmetric diamond anvil cell (DAC). The DAC is composed of one partially perforated diamond anvil opposing a minianvil mounted on a fully perforated diamond anvil with 1-mm culet diameter. A 250-μm stainless-steel gasket is preindented to a thickness of 120 μm and a 450-μm diameter hole is drilled for the sample chamber. The sample is loaded into the sample chamber along with gold powder and small ruby chips, which serve as pressure markers. Si oil is used as a pressure medium. Data are collected between ambient pressure and 25 kbar (2.5 GPa). Samples are measured at a wavelength of 0.416 46 Å and the lattice parameters are refined using the EXPGUI-GSAS software package [26].

The magnetostriction and thermal-expansion measurements in quasistatic fields are performed by using commercial strain gauges (SK-06-030TY-350, Vishay) glued to the sample surface with M-bond 610 adhesive. For better accuracy the strain gauge is connected to a Wheatstone bridge. The voltage-fed Wheatstone bridge is compensated before each measurement. Depending on the resistance change occurring in the strain gauges (due to the sample-length change) a corresponding voltage change of the bridge circuit is recorded by a DL750 oscilloscope.

Pulsed-field data are obtained at the Dresden High Magnetic Field Laboratory (HLD) [27]. The pulsed magnet used for magnetization and magnetostriction experiments can reach 60 T in about a 7-ms rise time, with a total pulse duration of about 25 ms. The magnetization is measured

utilizing a homebuilt pulsed-field magnetometer, described in Ref. [28], by integrating the voltage induced in compensated pickup coils surrounding the sample.

The magnetostriction in pulsed magnetic fields is measured by using an optical fiber strain gauge attached to the surface of the sample with cyanoacrylate epoxy. The strain gauge is a 1-mm-long fiber Bragg grating with a peak reflectivity at 1550 nm. A sample elongation is converted to a reflectivity-peak shift, which is detected by a high-resolution grating spectrometer providing $\Delta l/l$ resolution better than 5×10^{-7}. For more details, see Ref. [29].

Pulsed-field magnetocaloric measurements are performed using a pulsed magnet reaching up to 50 T with a 50-ms pulse duration. The thermocouple and sample mounting are similar to the static-field measurements. The sample is enclosed in a thin-walled shield, which is set under reduced pressure to provide better adiabaticity. The thermocouple signal is recorded by a storage oscilloscope.

III. RESULTS

A. Magnetization in static and pulsed fields

The magnetization of $LaFe_{11.74}Co_{0.13}Si_{1.13}$ measured in fields up to 14 T for different temperatures near the first-order transition ($T_C = 198$ K) are shown in Fig. 1(a). A field-induced transition from the PM to FM state is visible with a clear first-order character for all temperatures above 198 K. Characteristic S-shaped magnetization curves with hysteresis between up and down sweeps are observed. The hysteresis width decreases with increasing temperature and the transition is slightly broadened. The critical field of the transition increases with temperature at a rate of 0.25 T/K.

The inset of Fig. 1(a) shows magnetization data measured in pulsed fields up to 60 T. The 7-ms duration of the up sweep is too short to keep the sample at a constant temperature ensuring adiabatic conditions. Although the pulsed-field magnetization shows transitions with similar S shapes as the static-field data, the critical fields are higher than those for the isothermal magnetization process. One pulsed-field data set with an initial temperature $T_i = 198$ K is plotted as a black curve in Fig. 1(a) showing the difference between the isothermal and adiabatic magnetization data (black arrows).

This difference can be explained as follows: When the magnetic field approaches the critical value, the sample under adiabatic conditions starts heating up. The magnetization during the pulsed-field experiment then eventually reaches values of corresponding isotherms measured at $T_i + \Delta T_{ad}$. The latter is reflected by the length of the black arrows in Fig. 1. Comparing with ΔT_{ad} determined in our direct MCE measurements we find a reasonable agreement.

Figure 1(b) displays the isothermal magnetization of $LaFe_{11.21}Co_{0.65}Si_{1.11}$. Here, the magnetization increases smoothly with field without any sign of a first-order transition. Again, the pulsed-field data [inset of Fig. 1(b)]
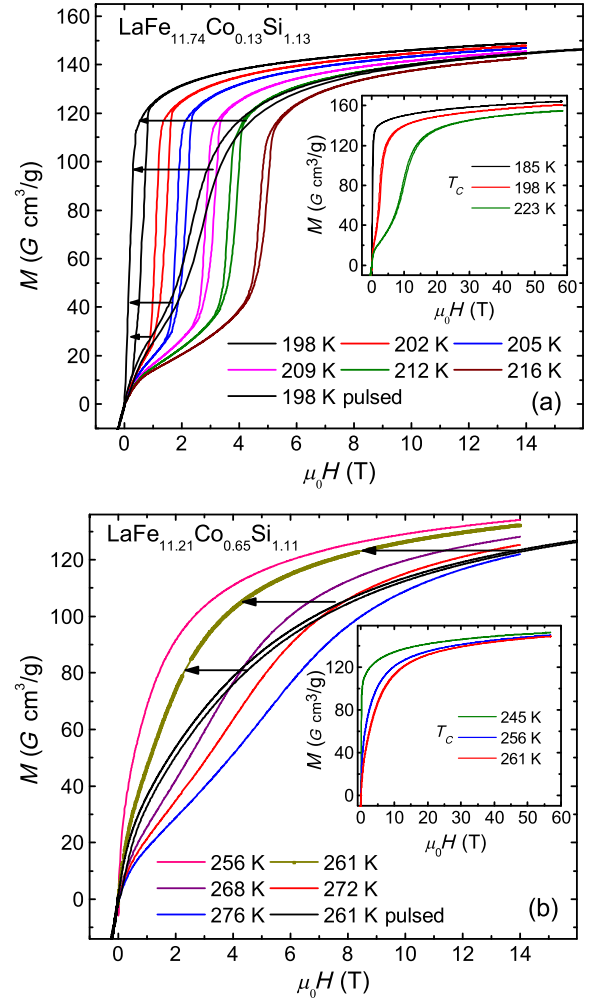

FIG. 1.   Field-dependent magnetization of (a) $LaFe_{11.74}Co_{0.13}Si_{1.13}$ and (b) $LaFe_{11.21}Co_{0.65}Si_{1.11}$. Colored lines show isothermal data measured in static magnetic fields. The insets show corresponding pulsed-field magnetization curves. The arrows depict the mismatch between the isothermal and the corresponding pulsed-field data (black curves).

can be considered as adiabatic magnetization. The black arrows in Fig. 1(b) indicate the corresponding temperature increase ΔT_{ad} that can be extracted from the isothermal magnetization. A comparison of adiabatic and isothermal magnetization curves can be used as an indirect technique for measuring the magnetocaloric effect [30].

B. Direct measurements of ΔT_{ad}

The inset of Fig. 2(a) shows the field-dependent ΔT_{ad} for $LaFe_{11.74}Co_{0.13}Si_{1.13}$ at $T_i = 188$ and 212 K recorded during a 10-T field pulse. Taking the values of such curves (down ramp) for different T_i and field strengths, the data shown in Fig. 2(a) are obtained. For 2 T, ΔT_{ad} shows a maximum of about 8 K at $T_i = 198$ K. For 5- and 10-T pulses, the maxima in ΔT_{ad} of about 11 and 13 K, respectively, are reached at somewhat higher initial
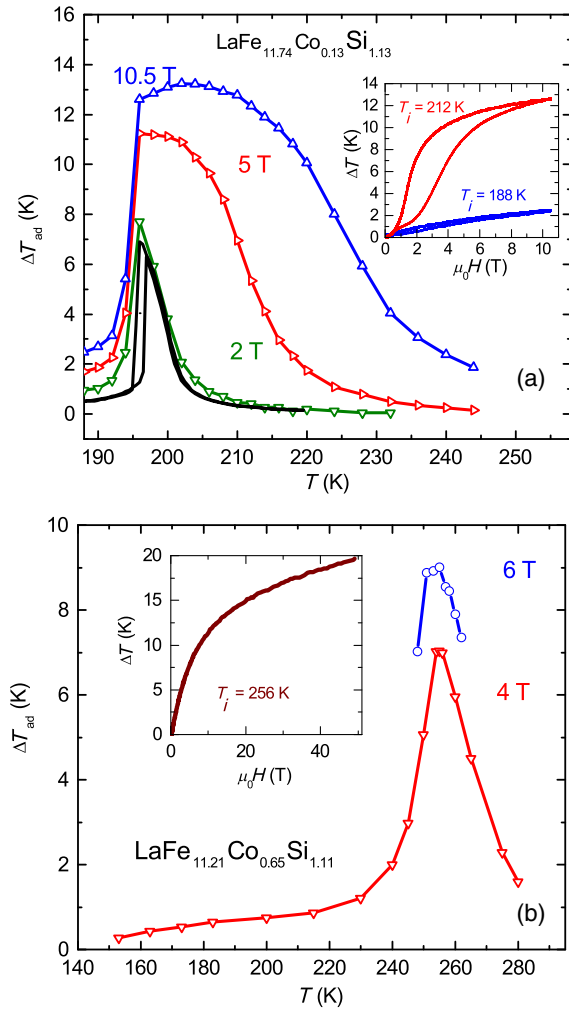
FIG. 2. Adiabatic temperature change ΔT_{ad} as a function of the initial temperature for (a) $LaFe_{11.74}Co_{0.13}Si_{1.13}$ and (b) $LaFe_{11.21}Co_{0.65}Si_{1.11}$. The black line in (a) corresponds to quasistatic measurements. The inset in (a) shows the field-dependent temperature change during 10 T field pulses for $T_i = 188$ and 212 K. The inset in (b) shows the field dependence of ΔT_{ad} for $T_i = T_C = 256$ K.

temperatures T_i. The black curve represents MCE data measured in quasistatic fields up to 1.8 T (Halbach setup).

The temperature dependence of ΔT_{ad} of $LaFe_{11.21}Co_{0.65}Si_{1.11}$ for 4- and 6-T pulses is shown in Fig. 2(b). ΔT_{ad} exhibits a sharp peak near T_C at 256 K with a maximum value of about 7 K (at 4 T). For 6-T pulses, the maximum in ΔT_{ad} increases to about 9 K. The inset to the figure shows the field dependence of ΔT_{ad} measured in a 50-T pulse for $T_i = T_C = 256$ K. The effect amounts to about 20 K.

Figure 3(a) shows the magnetic-field dependence of ΔT_{ad} for $LaFe_{11.74}Co_{0.13}Si_{1.11}$ in pulsed magnetic fields up to 50 T for various initial temperatures. The maximum of ΔT_{ad} is about 20 K for an initial temperature of 223 K. In order to better understand the physics behind this behavior,
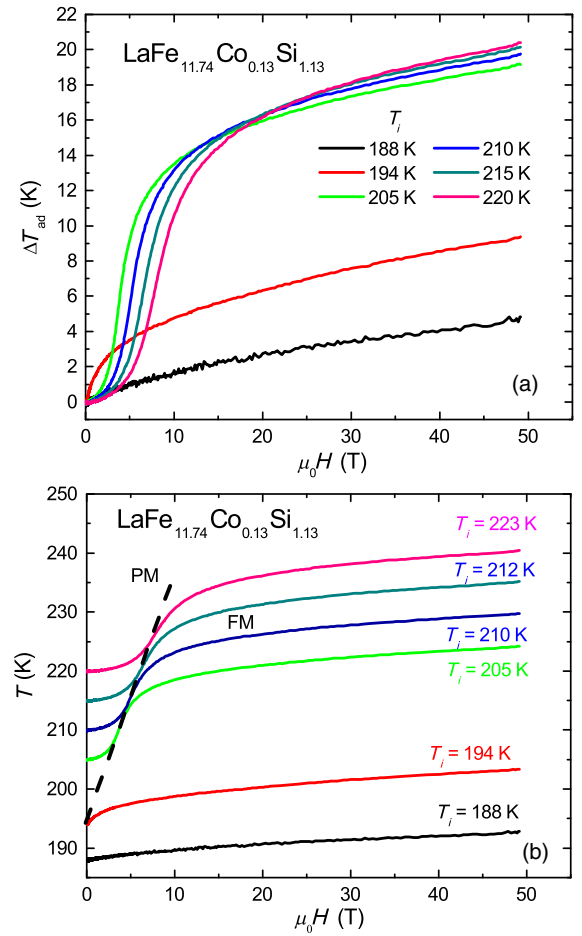

FIG. 3. (a) Field dependence of ΔT_{ad} of $LaFe_{11.74}Co_{0.13}Si_{1.11}$ measured in pulsed magnetic fields up to 50 T for various initial temperatures around T_C. (b) Field dependence of the sample temperature for different initial temperatures in pulsed fields.

the data are plotted as sample temperature vs applied magnetic field [Fig. 3(b)] [31]. The phase boundary separating the PM and FM states is drawn as a dashed line. When the magnetic field is applied at temperatures above the zero-field T_C (e.g., at 212 K), first, in the PM state, the entropy changes slightly and, consequently, a small temperature increase is observed. When entering the FM state a significant sample heating occurs. Beyond this phase transition, in the FM state, again the temperature increase becomes modest.

C. Magnetostriction

$La(Fe, Si, Co)_{13}$ compounds with first-order transitions exhibit a large volume change at their phase transitions [32,33]. This makes pulsed-field magnetostriction experiments highly challenging as the sample tends to establish cracks, even after an initial magnetization [34]. This can be ascribed not only to the volume change itself, but also to the fast field-sweep rate in pulsed magnetic fields, which increases the mechanical stress in the sample. A typical
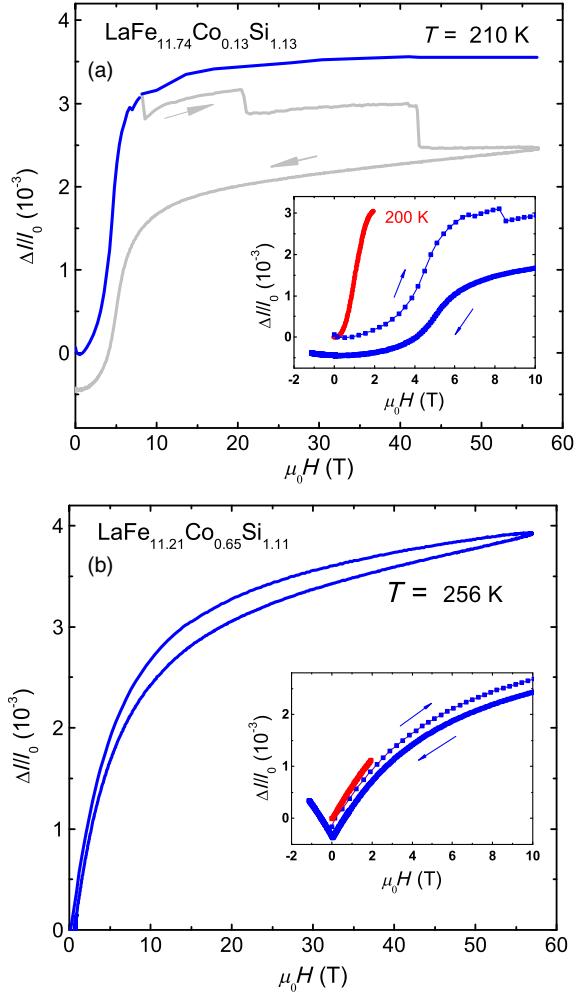
FIG. 4. Longitudinal magnetostriction $\Delta l/l_0$ measured at (a) 210 K for $LaFe_{11.74}Co_{0.13}Si_{1.13}$ and (b) 256 K for $LaFe_{11.21}Co_{0.65}Si_{1.11}$. The insets display the pulsed-field data together with the static-field data.

result of a pulsed-field magnetostriction experiment of a $LaFe_{11.74}Co_{0.13}Si_{1.13}$ sample at 210 K is shown in Fig. 4(a). (All magnetostriction measurements are performed in longitudinal configuration, i.e., with the field parallel to the length change.) The abrupt steps in $\Delta l/l_0$ are the result of sample cracks (gray curve). The undisturbed magnetostriction is approximated by moving the affected data blocks upward (blue curve). This approach can be justified when comparing to static-field data. Magnetostriction measurements in static fields face similar difficulties due to sample cracks. However, one successful static-field measurement without the appearance of cracks is shown in the inset of Fig. 4(a). Since here the maximum field is 2 T, the measurement is performed at $T_i = 200$ K, i.e., closer to T_C, allowing us to complete the transition within the given field range. The static-field data are close to saturation at 2 T. Accordingly, the pulsed-field data at 210 K has almost reached saturation at $\Delta l/l_0 = 0.35\%$ before the first crack appeared. This supports the

reconstructed pulsed-field magnetostriction to be correct. Similar to the magnetization data, the magnetostriction shows a sharp increase due to the first-order transition with a hysteresis width of about 1.5 T. Assuming a uniform magnetovolume effect in our cubic systems [35], we estimate a volume increase of about 1%.

The longitudinal magnetostriction of $LaFe_{11.21}Co_{0.65}Si_{1.11}$, on the other hand, shows a smooth increase of the sample length at 256 K [Fig. 4(b)]. This is reminiscent of the magnetization data [Fig. 1(b)]. The maximum in $\Delta l/l_0$ of about 0.4% is somewhat larger than for the former compound. The magnetostriction measured in pulsed and static fields for the same initial temperature show very good agreement [inset of Fig. 4(b)].

High-pressure XRD experiments are carried out on the $LaFe_{11.74}Co_{0.13}Si_{1.13}$ sample above its Curie temperature ($T = 260$ K, data not shown) to obtain the sample compressibility. The fit of the pressure-dependent volume to a second-order Birch-Murnaghan equation of state [36] yields $K = (0.999 \pm 0.015) \times 10^{-12}$ cm^2/dyne. This value is reproduced within error in independent measurements using acoustic techniques, which yields $K = (1.070 \pm 0.016) \times 10^{-12}$ cm^2/dyne for the $LaFe_{11.21}Co_{0.65}Si_{1.11}$ sample.

IV. DISCUSSION

The itinerant nature of the magnetism in $La(FeCoSi)_{13}$ compounds is defined by the density of states at the Fermi level $N(E_F)$. Band-structure calculations for the undoped system have been performed by Fujita *et al.* [37]. The different magnetic properties in the compounds are rather easy to understand qualitatively in terms of the band filling. Co has one additional $3d$ electron compared to Fe, so Co acts as an electron dopant. As the $3d$ bands are quite evolved, the additional band filling may have a complex influence on $N(E_F)$. If $N(E_F)$ is large enough, the Stoner criterion is fulfilled, and the system becomes ferromagnetic at a second-order T_C. In case the Stoner criterion is not fulfilled, but is close to that, a positive curvature of $N(E)$ can lead to metamagnetic behavior. Our results are consistent with this scenario at low fields. Interestingly, at high fields, this difference tends to vanish. At fields of the order of 50 T, the thermodynamic properties are about equal: The magnetization of both compounds converges to about 160 G cm^3/g, ΔT_{ad} reaches about 20 K, and the linear magnetostriction saturates at ~0.35%. Apparently, if the applied field is large enough, differences in the specific shape of $N(E)$ are no longer important.

Obviously, the difference at low fields is due to the first-order field-induced (metamagnetic) transition, present for the Co-poor compound. The transition leads not only to the magnetization jump, but also to the huge volume increase which is inherent to the transition. Such a behavior is well described by the phenomenological theory proposed by Bean and Rodbell [23]. This theory assumes a linear dependence of T_C on the sample volume,

$$T_C = T_0(1 + \beta\omega), \tag{1}$$

where $\omega = (V - V_0)/V_0$. Following the notation of Ref. [23], T_0 is the Curie temperature if the sample would be incompressible, V_0 is the corresponding volume in the absence of exchange interactions, and β is the slope of the T_C dependence on volume. Minimizing the corresponding potential and setting the external pressure to zero, one obtains

$$\omega = \frac{1}{2}NKk_BT_0\beta\left(\frac{M}{M_s}\right)^2, \tag{2}$$

where N is the number of atoms per unit volume, K is the compressibility, k_B is the Boltzmann constant, and M_S is the saturation magnetization. At this point, it is worth noting that Eq. (1) is the only assumption here, no restriction has been set concerning the origin of the magnetism. Equation (2) shows that in the framework of the Bean-Rodbell model the relative volume change ω is proportional to the magnetization squared. The coefficient $NKk_BT_0\beta/(2M_s^2)$ can then easily be found using a plot of ω vs M^2 (Fig. 5).
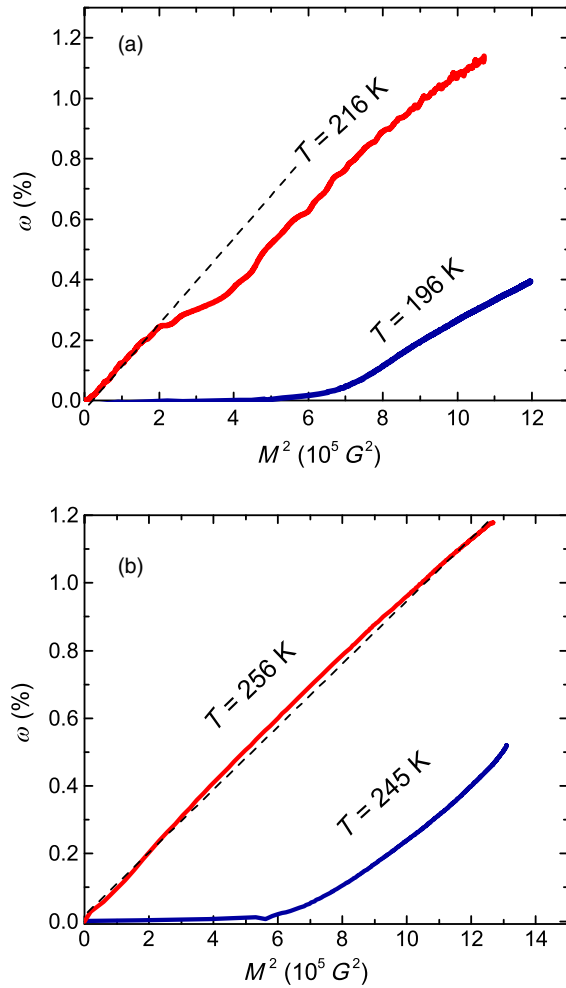

FIG. 5. Magnetostriction vs squared magnetization plotted for temperatures below and above T_C for (a) LaFe$_{11.74}$Co$_{0.13}$Si$_{1.13}$ and (b) LaFe$_{11.21}$Co$_{0.65}$Si$_{1.11}$.

In order to check the applicability of the theory we plotted $\omega = 3\Delta l/l$ (assuming isotropic expansion) of both samples against the magnetization squared in Fig. 5. For the sample with second-order transition [Fig. 5(b)], a clear linear dependence is observed above T_C. The curve below T_C at 245 K is not linear anymore, as exchange fields should be taken into account. Some groups [37–39] point out that Eq. (2) should be extended to take into account spin fluctuations. This correction seems to be insignificant for our discussion. The Co-poor sample with first-order transition shows as well a linear dependence in ω vs M^2 above T_C at 216 K until the metamagnetic transition appears [Fig. 5(a)]. Below T_C at 196 K again nonlinearity is observed. These results show that in both compounds the magnetization is intrinsically connected to the expansion. This explains the concurrence of the thermodynamic parameters at high fields.

A general local-moment volume magnetostriction theory was developed by Callen and Callen [40]. They showed that the spontaneous volume magnetostriction is proportional to the squared magnetization, compressibility, and magnetovolume coupling constant Γ,

$$\omega = K\Gamma M^2. \tag{3}$$

A similar equation was obtained by Shimizu [41] by extending the Wohlfarth model [42] for itinerant ferromagnets with volume-dependent terms (see also Ref. [39]). By using this approach Palstra *et al.* [43] report $K\Gamma = 1.71$–1.79×10^{-8} G^{-2} for La(Fe$_{1-x}$Al$_x$)$_{13}$ alloys with first-order metamagnetic transitions. In our experiments, we obtain $K\Gamma = 1.12 \times 10^{-8}$ G^{-2} for LaFe$_{11.74}$Co$_{0.13}$Si$_{1.13}$ and $K\Gamma = 0.91 \times 10^{-8}$ G^{-2} for LaFe$_{11.21}$Co$_{0.65}$Si$_{1.11}$ (Fig. 5).

One of the important results of the Bean-Rodbell theory is the criterion to distinguish first- and second-order transitions. If the parameter

$$\eta \equiv C_JNKk_BT_0\beta^2 \tag{4}$$

is larger than 1, the transition is first order, for $0 < \eta < 1$ a second-order transition is observed. It has to be mentioned that this criterion is derived in the frame of a mean-field model, where the entropy is given by the direct application of the Boltzmann definition [44]. The coefficient C_J depends on the quantum spin number J, or, otherwise, on the moment of the magnetic atom. The magnetism of our compounds is, however, clearly of an itinerant nature, where a simple analytical expression of the magnetic entropy is not possible. We limit ourselves to temperatures well above T_C, where the inverse susceptibility is linear in temperature according to both itinerant and localized models.

The temperature dependence of the inverse magnetic susceptibility for both alloys is shown in Fig. 6. The extrapolated Curie-Weiss temperature $T_0 = 256$ K for the

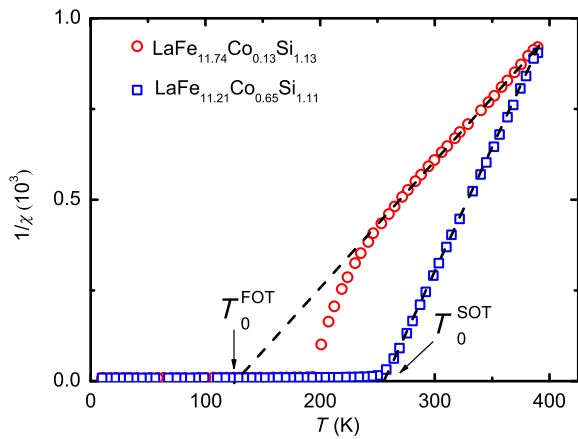FIG. 6.   Inverse magnetic susceptibility of $LaFe_{11.74}Co_{0.13}Si_{1.13}$ (first-order transition, FOT) and $LaFe_{11.21}Co_{0.65}Si_{1.11}$ (second-order transition, SOT). Dashed lines are linear extrapolations from the high-temperature data for the determination of T_0.

material with second-order transition corresponds to the observed Curie temperature, whereas for the alloy with first-order transition $T_0 = 125$ K is significantly lower than T_C. From the Curie-Weiss fits, we obtain effective moments of about $1.4\mu_B$ per Fe atom for $LaFe_{11.74}Co_{0.13}Si_{1.13}$ and about $1\mu_B$ for $LaFe_{11.21}Co_{0.65}Si_{1.11}$ [45]. The corresponding values of C_J are 1.3 and 0.8. From Eqs. (2) and (4) we obtain for the compound with first-order transition $\beta = 28$ and $\eta = 1.2$. This value is just above unity, which agrees with the fact that the observed hysteresis is quite narrow. The corresponding values for the Co-rich compound are $\beta = 10$ and $\eta = 0.3$. Hence, a second-order transition is expected as it is observed.

It has to be mentioned that determining of the order of the transition is possible as well by purely magnetic methods, for example, using the Arrott plot (M^2 against B/M) [46,47], where the order of the transition is determined by the sign of the slope, or the sign of the M^4 coefficient in the free-energy expansion. The Bean-Rodbell theory instead takes into account the dependence of the exchange interactions on interatomic distances, and properly describes magnetovolume instabilities leading to a first-order transition. In this manner, not only the order of the transition is determined, but the behavior of the system in the vicinity of the tricritical point is described.

In conclusion, we have performed magnetization, magnetostriction, and magnetocaloric-effect measurements in magnetic fields up to 60 T for $LaFe_{11.74}Co_{0.13}Si_{1.13}$ and $LaFe_{11.21}Co_{0.65}Si_{1.11}$. The former shows a first-order metamagnetic transition with abrupt increase of magnetization and volume in fields up to 5 T. The transition is accompanied by a substantial heat release. $LaFe_{11.21}Co_{0.65}Si_{1.11}$, on the other hand, does not show a metamagnetic behavior and, above the Curie temperature, is an ordinary paramagnet. The magnetocaloric effect reaches about 20 K at 50 T in both compounds. We are able to quantify the magnetoelastic coupling and, based on that, apply the Bean and Rodbell criterion distinguishing first- and second-order transitions.

[1] A. M. Tishin and Y. I. Spichkin, *The Magnetocaloric Effect and Its Applications* (Institute of Physics Publishing, Bristol and Philadelphia, 2003).

[2] O. Gutfleisch, M. A. Willard, E. Bruck, C. H. Chen, S. G. Sankar, and J. P. Liu, Magnetic materials and devices for the 21st century: Stronger, lighter, and more energy efficient, Adv. Mater. **23,** 821 (2011).

[3] E. Brück, in *Handbook of Magnetic Materials*, edited by K. H. J. Buschow (Elsevier, North-Holland, Amsterdam, 2008), Vol. 17, Chap. 4, pp. 235.

[4] K. A. Gschneidner, Jr. and V. K. Pecharsky, Thirty years of near room temperature magnetic cooling: Where we are today and future prospects, Int. J. Refrig. **31,** 945 (2008).

[5] C. Zimm, A. Jastrab, A. Sternberg, V. Pecharsky, K. A. Gschneidner, Jr., M. Osborne, and I. Anderson, Description and performance of a near-room temperature magnetic refrigerator, Adv. Cryog. Eng. **43,** 1759 (1998).

[6] A. Kitanovski, J. Tušek, U. Tomc, U. Plaznik, M. Ozbolt, and A. Poredoš, *Magnetocaloric Energy Conversion* (Springer, Switzerland, 2015), Chap. 7, pp. 269–330.

[7] A. Kitanovski and P. W. Egolf, Thermodynamics of magnetic refrigeration, Int. J. Refrig. **29,** 3 (2006).

[8] K. P. Skokov, A. Yu. Karpenkov, D. Yu. Karpenkov, and O. Gutfleisch, The maximal cooling power of magnetic and thermoelectric refrigerators with La(FeCoSi)$_{13}$ alloys, J. Appl. Phys. **113,** 17A945 (2013).

[9] K. G. Sandeman, Magnetocaloric materials: The search for new systems, Scr. Mater. **67,** 566 (2012).

[10] V. K. Pecharsky, K. A. Gschneidner, Jr., A. O. Pecharsky, and A. M. Tishin, Thermodynamics of the magnetocaloric effect, Phys. Rev. B **64,** 144406 (2001).

[11] K. P. Skokov, K.-H. Müller, J. D. Moore, J. Liu, A. Yu. Karpenkov, M. Krautz, and O. Gutfleisch, Influence of

thermal hysteresis and field cycling on the magnetocaloric effect in $LaFe_{11.6}Si_{1.4}$, J. Alloys Compd. **552,** 310 (2013).

[12] T. Gottschall, K. P. Skokov, R. Burriel, and O. Gutfleisch, On the $S(T)$ diagram of magnetocaloric materials with first-order transition: Kinetic and cyclic effects of Heusler alloys, Acta Mater. **107,** 1 (2016).

[13] J. Liu, T. Gottschall, K. P. Skokov, J. D. Moore, and O. Gutfleisch, Giant magnetocaloric effect driven by structural transitions, Nat. Mater. **11,** 620 (2012).

[14] F. Cugini, G. Porcari, C. Viappiani, L. Caron, A. O. dos Santos, L. P. Cardoso, E. C. Passamani, J. R. C. Proveti, S. Gama, E. Brück, and M. Solzi, Millisecond direct measurement of the magnetocaloric effect of a Fe_2P-based compound by the mirage effect, Appl. Phys. Lett. **108,** 012407 (2016).

[15] V. V. Khovaylo, K. P. Skokov, O. Gutfleisch, H. Miki, R. Kainuma, and T. Kanomata, Reversibility and irreversibility of magnetocaloric effect in a metamagnetic shape memory alloy under cyclic action of a magnetic field, Appl. Phys. Lett. **97,** 052503 (2010).

[16] A. Chirkova, K. P. Skokov, L. Schultz, N. V. Baranov, O. Gutfleisch, and T. G. Woodcock, Giant adiabatic temperature change in FeRh alloys evidenced by direct measurements under cyclic conditions, Acta Mater. **106,** 15 (2016).

[17] O. Gutfleisch, T. Gottschall, M. Fries, D. Benke, I. Radulov, K. P. Skokov, H. Wende, M. Gruner, M. Acet, P. Entel, and M. Farle, Mastering hysteresis in magnetocaloric materials, Phil. Trans. R. Soc. A **374,** 0308 (2016).

[18] L. Morellon, Z. Arnold, C. Magen, C. Ritter, O. Prokhnenko, Y. Skorokhod, P. A. Algarabel, M. R. Ibarra, and J. Kamarad, Pressure Enhancement of the Giant Magnetocaloric Effect in $Tb_5Si_2Ge_2$, Phys. Rev. Lett. **93,** 137201 (2004).

[19] K. Morrison, J. D. Moore, K. G. Sandeman, A. D. Caplin, and L. F. Cohen, Capturing first- and second-order behavior in magnetocaloric $CoMnSi_{0.92}Ge_{0.08}$, Phys. Rev. B **79,** 134408 (2009).

[20] S. Fujieda, Y. Hasegawa, A. Fujita, and K. Fukamichi, Thermal transport properties of magnetic refrigerants $La(Fe_xSi_{1-x})_{13}$ and their hydrides, and $Gd_5Si_2Ge_2$ and MnAs, J. Appl. Phys. **95,** 2429 (2004).

[21] F. X. Hu, J. Gao, X. L. Qian, M. Ilyn, A. M. Tishin, J. R. Sun, and B. G. Shen, Magnetocaloric effect in itinerant electron metamagnetic systems, J. Appl. Phys. **97,** 10M303 (2005).

[22] J. Liu, J. D. Moore, K. P. Skokov, M. Krautz, K. Löwe, A. Barcza, M. Katter, and O. Gutfleisch, Exploring $La(Fe,Si)_{13}$-based magnetic refrigerants towards application, Scr. Mater. **67,** 584 (2012).

[23] C. P. Bean and D. S. Rodbell, Magnetic disorder as a first-order phase transformation, Phys. Rev. **126,** 104 (1962).

[24] B. R. Hansen, L. T. Kuhn, C. R. H. Bahl, M. Lundberg, C. Ancona-Torres, and M. Katter, Properties of magnetocaloric $La(Fe,Co,Si)_{13}$ produced by powder metallurgy, J. Magn. Magn. Mater. **322,** 3447 (2010).

[25] M. Katter, V. Zellmann, G. Reppel, and K. Uestuener, Magnetocaloric properties of $La(Fe,Co,Si)_{13}$ bulk material prepared by powder metallurgy, IEEE Trans. Magn. **44,** 3044 (2008).

[26] B. H. Toby, EXPGUI, a graphical user interface for GSAS, J. Appl. Crystallogr. **34,** 210 (2001).

[27] S. Zherlitsyn, B. Wustmann, T. Herrmannsdörfer, and J. Wosnitza, Status of the pulsed-magnet-development program at the Dresden High Magnetic Field Laboratory, IEEE Trans. Appl. Supercond. **22,** 4300603 (2012).

[28] Y. Skourski, M. D. Kuz'min, K. P. Skokov, A. V. Andreev, and J. Wosnitza, High-field magnetization of Ho_2Fe_{17}, Phys. Rev. B **83,** 214420 (2011).

[29] R. Daou, F. Weickert, M. Nicklas, F. Steglich, A. Haase, and M. Doerr, High resolution magnetostriction measurements in pulsed magnetic fields using fiber Bragg gratings, Rev. Sci. Instrum. **81,** 033909 (2010).

[30] R. Z. Levitin, V. V. Snegirev, A. V. Kopylov, A. S. Lagutin, and A. Gerber, Magnetic method of magnetocaloric effect determination in high pulsed magnetic fields, J. Magn. Magn. Mater. **170,** 223 (1997).

[31] K. P. Skokov, V. V. Khovaylo, K.-H. Müller, J. D. Moore, J. Liu, and O. Gutfleisch, Magnetocaloric materials with first-order phase transition: Thermal and magnetic hysteresis in $LaFe_{11.8}Si_{1.2}$ and $Ni_{2.21}Mn_{0.77}Ga_{1.02}$, J. Appl. Phys. **111,** 07A910 (2012).

[32] A. Fujita, K. Fukamichi, J.-T. Wang, and Y. Kawazoe, Large magnetovolume effects and band structure of itinerant-electron metamagnetic $La(Fe_xSi_{1-x})_{13}$ compounds, Phys. Rev. B **68,** 104431 (2003).

[33] A. K. Pathak, P. Basnyat, I. Dubenko, S. Stadler, and N. Ali, Magnetic, magnetocaloric, and magnetoelastic properties of compounds, J. Appl. Phys. **106,** 063917 (2009).

[34] A. Waske, L. Giebeler, B. Weise, A. Funk, M. Hinterstein, M. Herklotz, K. Skokov, S. Fahler, O. Gutfleisch, and J. Eckert, Asymmetric first-order transition and interlocked particle state in magnetocaloric $La(Fe,Si)_{13}$, Phys. Status Solidi RRL **9,** 136 (2015).

[35] A. Fujita, S. Fujieda, Y. Hasegawa, and K. Fukamichi, Itinerant-electron metamagnetic transition and large magnetocaloric effects in $La(Fe_xSi_{1-x})_{13}$ compounds and their hydrides, Phys. Rev. B **67,** 104416 (2003).

[36] F. Birch, Finite strain isotherm and velocities for single-crystal and polycrystalline NaCl at high pressures and 300 K, J. Geophys. Res. **83,** 1257 (1978).

[37] A. Fujita, K. Fukamichi, M. Yamada, and T. Goto, Influence of pressure on itinerant electron metamagnetic transition in compound, J. Appl. Phys. **93,** 7263 (2003).

[38] H. Yamada, Pressure effect in an itinerant-electron metamagnet at finite temperature, J. Magn. Magn. Mater. **139,** 162 (1995).

[39] T. Moriya and K. Usami, Magneto-volume effect and invar phenomena in ferromagnetic metals, Solid State Commun. **34,** 95 (1980).

[40] E. C. Callen and H. B. Callen, Magnetostriction, Forced Magnetostriction, and Anomalous Thermal Expansion in Ferromagnets, Phys. Rev. **139,** A455 (1965).

[41] M. Shimizu, Magnetovolume effects in itinerant electron ferromagnets, J. Magn. Magn. Mater. **20,** 47 (1980).

[42] E. P. Wohlfarth, Forced magnetostriction in the band model of magnetism, J. Phys. C **2,** 68 (1969).

[43] T. T. M. Palstra, G. J. Nieuwenhuys, J. A. Mydosh, and K. H. J. Buschow, Mictomagnetic, ferromagnetic, and antiferromagnetic transitions in $La(Fe_xAl_{1-x})_{13}$ intermetallic compounds, Phys. Rev. B **31,** 4622 (1985).

[44] J. S. Smart, Magnetic structure transitions, Phys. Rev. **90**, 55 (1953).

[45] The same approach was used in the original paper of Bean and Rodbell [23] to obtain the spin quantum number of Mn in MnAs.

[46] S. K. Banerjee, On a generalised approach to first and second order magnetic transitions, Phys. Lett. **12**, 16 (1964).

[47] H. Yamada, Metamagnetic transition and susceptibility maximum in an itinerant-electron system, Phys. Rev. B **47**, 11211 (1993).